



Article

Investigation of the Performance of Hyperspectral Imaging by Principal Component Analysis in the Prediction of Healing of Diabetic Foot Ulcers

Qian Yang ¹, Shen Sun ², William J. Jeffcoate ³, Daniel J. Clark ³, Alison Musgove ³ ,
Fran L. Game ⁴ and Stephen P. Morgan ^{1,*} 

¹ Optics and Photonics Research Group, Faculty of Engineering, University of Nottingham, Nottingham NG7 2RD, UK; eexqy3@icloud.com

² Biomedical Information Processing Lab, College of Life Science and Bioengineering, Beijing University of Technology, Beijing 100124, China; sunshen@bjut.edu.cn

³ Nottingham University Hospitals NHS Trust, Nottingham NG5 1PB, UK; william.jeffcoate@gmail.com (W.J.J.); daniel.clark@nuh.nhs.uk (D.J.C.); awlmusgrove@hotmail.co.uk (A.M.)

⁴ University Hospitals of Derby and Burton NHS Foundation Trust, Derby DE22 3NE, UK; frances.game@nhs.net

* Correspondence: steve.morgan@nottingham.ac.uk; Tel.: +44-115-951-5570

Received: 22 September 2018; Accepted: 4 December 2018; Published: 7 December 2018



Abstract: Diabetic foot ulcers are a major complication of diabetes and present a considerable burden for both patients and health care providers. As healing often takes many months, a method of determining which ulcers would be most likely to heal would be of great value in identifying patients who require further intervention at an early stage. Hyperspectral imaging (HSI) is a tool that has the potential to meet this clinical need. Due to the different absorption spectra of oxy- and deoxyhemoglobin, in biomedical HSI the majority of research has utilized reflectance spectra to estimate oxygen saturation (SpO₂) values from peripheral tissue. In an earlier study, HSI of 43 patients with diabetic foot ulcers at the time of presentation revealed that ulcer healing by 12 weeks could be predicted by the assessment of SpO₂ calculated from these images. Principal component analysis (PCA) is an alternative approach to analyzing HSI data. Although frequently applied in other fields, mapping of SpO₂ is more common in biomedical HSI. It is therefore valuable to compare the performance of PCA with SpO₂ measurement in the prediction of wound healing. Data from the same study group have now been used to examine the relationship between ulcer healing by 12 weeks when the results of the original HSI are analyzed using PCA. At the optimum thresholds, the sensitivity of prediction of healing by 12 weeks using PCA (87.5%) was greater than that of SpO₂ (50.0%), with both approaches showing equal specificity (88.2%). The positive predictive value of PCA and oxygen saturation analysis was 0.91 and 0.86, respectively, and a comparison by receiver operating characteristic curve analysis revealed an area under the curve of 0.88 for PCA compared with 0.66 using SpO₂ analysis. It is concluded that HSI may be a better predictor of healing when analyzed by PCA than by SpO₂.

Keywords: hyperspectral imaging; principal component analysis; oxygen saturation; wound healing; diabetic foot ulcer

1. Introduction

Diabetic foot ulcers are thought to affect 15–25% of people with diabetes during their lifetime [1] and are a major source of suffering and cost. The principal pathological conditions contributing to foot ulceration are peripheral neuropathy, peripheral artery disease, pre-existing deformity, and trauma,

but the contributions of each vary considerably. While some ulcers heal relatively quickly, others fail to heal and deteriorate. An accurate prediction of those ulcers least likely to heal quickly can therefore be useful, because it would enable consideration of more intensive intervention at an earlier stage and thereby improve overall outcome.

Peripheral artery disease can both cause ulceration and delay its healing by reducing the delivery of oxygen to peripheral tissues. While there are a number of approaches to assessing the extent of disease in larger arteries (including pulse palpation, pressure measurements, and angiography), none are routinely used to investigate associated dysfunction of smaller arteries, arterioles, and capillaries. One option that has been explored is hyperspectral imaging (HSI).

HSI is a noninvasive technique by which images are formed at different wavelengths to produce a hypercube (x, y, λ). Due to the different absorption spectra of oxy- and deoxyhemoglobin, in biomedical HSI the majority of research has utilized the reflectance hypercube to estimate oxygen saturation (SpO_2) values from peripheral tissue [2–9].

Greenman and colleagues used HSI to investigate whether oxygen delivery and muscle metabolism were factors in diabetic foot disease. That study included 108 individuals without ulceration, comparing three groups: volunteers without diabetes, diabetic patients without neuropathy, and patients with both diabetes and neuropathy [5]. SpO_2 was reduced in people with diabetes, and especially in those with neuropathy. Yudovsky et al. [6] also used HSI in the visible spectrum (450–700 nm) to predict tissue breakdown. A two-layer (epidermis, dermis) skin model was used to fit to the measured data and obtain an index of SpO_2 . The algorithm was able to predict tissue at risk of ulceration with a sensitivity and specificity of 95% and 80% respectively, 58 days before breakdown is visible to the naked eye [6].

A formula to derive an indication of SpO_2 from HSI was also used by Khaodhiar et al. [7] to estimate oxyhemoglobin and deoxyhemoglobin of 10 patients with type 1 diabetes with foot ulcers, 13 without ulcers, and 14 subjects without diabetes. A spectrum for each pixel was compared with standard tissue to determine measures of oxyhemoglobin and deoxyhemoglobin. Using this approach, the sensitivity and specificity of HSI in predicting ulcer healing were 93% and 86%, while the positive and negative predictive values for ulceration were calculated as 93% and 86%. Nouvong et al. [8] used a similar approach to estimate relative values of tissue oxyhemoglobin and deoxyhemoglobin in 66 people with diabetic foot ulcers and reported that the sensitivity of HSI to predict healing within 6 months was 80% and the specificity was 74%. As discussed in our previous work [9], both of these papers had weaknesses, which helps to explain the differences between results of [7–9]. The first study [7] was very small and acknowledged to be simply a pilot, and both studies based their analysis on outcome per ulcer rather than outcome per person. The population included in the second study [8] was also highly selected, with a mean age of participants of just over 50 years, much younger than a representative population with diabetic foot ulcers.

Principal component analysis (PCA) is an alternative approach to analyzing HSI data. Although frequently applied in other fields, such as remote sensing and the food industry, mapping of SpO_2 is more common in biomedical HSI. It is therefore valuable to compare the performance of PCA with SpO_2 measurement in the prediction of wound healing. PCA is a process that converts a number of possibly correlated variables into a set of linearly uncorrelated variables called principal components. PCA has been demonstrated to be an effective and efficient preprocessing method, as retaining only the first few principal components significantly reduces data [10]. In the food industry, PCA and HSI have been applied to tea classification [11], detection of bruise damage on mushrooms [12], and estimation of the quality of pork [13]. Some examples of the application of PCA in in vivo biomedical HSI are provided in useful reviews [14–16], with a focus on laparoscopic imaging [11,12]. PCA has also been used as a dimension-reduction algorithm for wavelet-based segmentation of hyperspectral colon tissue imagery [17]. For tissue measurement, the contiguous bands of a hypercube are highly correlated, as they are dominated by the oxy- and deoxyhemoglobin spectra. This has the benefit of being a data-reduction method for the hypercubes obtained from the tissues of feet affected by ulcers.

This study performed a novel investigation by comparing the performance of PCA with more widely used SpO₂ measurements in predicting whether a wound will heal within 12 weeks of presentation. More accurate prediction of wound healing will support earlier intervention and better treatment.

2. Method

2.1. Experimental Setup

The HSI setup is shown in Figure 1. Illumination of the foot was via 16 × 1 W white light-emitting diodes (LEDs) (LXHL-MWEC, Lumileds™ Lighting, San Jose, CA, USA) with 8 units placed on either side of the camera. Light scattered from the foot was passed through an aperture, which controlled the amount of collected light and was focused onto a detector by a C-mount lens (f = 15 mm, f# = 2.2; Schneider).

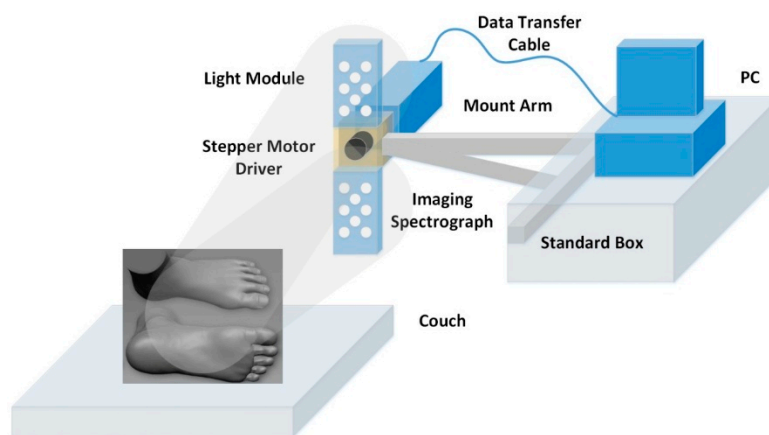


Figure 1. Hyperspectral imaging setup for imaging the foot (foot-to-lens distance typically 25–30 cm).

The HSI camera is a “push-broom” type that images a line from the scene onto a diffraction grating, which splits the light into a range of colors across the photosensor array. The camera comprises a Peltier cooled charge-coupled device (CCD) (Sensicam QE, PCO imaging, Cooke Corporation, Auburn Hills, MI, USA) coupled to an imaging spectrograph (ImSpector V10E, Specim Ltd., Oulu, Finland), which contains an input slit and a prism–grating–prism system. The input slit defines the field of view for the spatial scan, while the prism–grating–prism diffracts the light from the aperture into its spectrum. Scanning the line allows a 3D data cube that is transmitted to a PC via a peripheral component interface (PCI) for storage and future analysis. For the measurements taken in this study, each 3D data cube contained 2D spatial images (120 × 170 pixels) over a wavelength range from 430 nm to 750 nm (272 values). The sweep of the system moves from heel to toe and takes ~30 s to obtain an image, with an exposure time of 100 ms per row. Calibration images of white (99% reflectance Spectralon; Labsphere, Inc., North Sutton, NH, USA) and black (lens cap on camera) targets are recorded to take into account the effects of the nonuniform spectrum of the light source and dark noise, respectively. In order to reduce noise but not lose significant features in the reflected light spectra, a 9 point moving average filter is applied to the spectra.

For a certain position in the image plane (x, y) at a wavelength λ, the calibrated attenuation value is calculated as:

$$A(x, y, \lambda) = -\log \frac{I_{\text{sample}}(x, y, \lambda) - I_{\text{dark}}(x, y, \lambda)}{I_{\text{white}}(x, y, \lambda) - I_{\text{dark}}(x, y, \lambda)} \quad (1)$$

where I_{sample} is the intensity measured from the raw image, and I_{white} and I_{dark} are the intensities of the white and dark references, respectively.

2.2. Clinical Protocol

The data used to compare prediction of wound healing via SpO₂ and PCA were obtained in a clinical study described previously [9]. The published study received research ethics approval and all participants provided written informed consent. Recruitment was of a consecutive cohort, and the only major prespecified exclusions were those with a unilateral major amputation and those who withheld or were unable to give informed consent [9]. There was therefore no control of gender balance, as one would expect a predominance of male patients in all studies of foot ulcers. There was also no control of diabetes type, as this is not a recognized significant factor associated with the outcome of diabetic foot ulcers.

Participants attending an imaging session were required to avoid drinking tea or coffee and smoking tobacco for at least 2 hours prior to the visit, as these stimulants could lead to a change in blood flow. Capillary glucose was determined on arrival, and patients who were hypoglycemic were excluded from the study. All the studies were undertaken in a temperature-controlled clinic room at 22 °C and the test time was between 09:00 and 12:00. Prior to any assessments, participants lay on an examination couch for at least 15 minutes after removing their shoes and socks. Intensity hypercubes of the ulcer site were obtained for each participant, and the data were processed using SpO₂ algorithms and PCA, as described in Sections 2.3 and 2.4, respectively.

2.3. SpO₂ Data Processing

Oxygen saturation is defined as:

$$SpO_2 = \frac{HbO_2}{HbO_2 + Hb} \times 100\% \quad (2)$$

where *HbO₂* is the concentration of oxyhemoglobin (mole L⁻¹) and *Hb* is the concentration of deoxyhemoglobin (mole L⁻¹).

Due to the different absorption spectra of the dominant absorbers, oxy- and deoxyhemoglobin, it is possible to extract information about the oxygen saturation of tissues based on optical measurements such as HSI.

The absorption coefficient ($\mu_a(\lambda)$) and attenuation ($A(\lambda)$) can be expressed as [18]:

$$\mu_a(\lambda) = \alpha(\lambda)[HbO_2] + \beta(\lambda)[Hb] \quad (3)$$

$$A(\lambda) = (\alpha(\lambda)[HbO_2] + \beta(\lambda)[Hb])d \quad (4)$$

where $\alpha(\lambda)$ is the specific absorption of oxyhemoglobin (cm⁻¹ mole⁻¹ L), $\beta(\lambda)$ is the specific absorption of deoxyhemoglobin (cm⁻¹ mole⁻¹ L), and *d* is the path length of the light (cm).

If $\mu_a(\lambda)$ is known at 2 wavelengths, then it is straightforward to calculate SpO₂ from Equations (3) and (2), as $\alpha(\lambda)$ and $\beta(\lambda)$ are known from literature values. A challenge is to relate measurements of $A(\lambda)$ and $\mu_a(\lambda)$. In the absence of light scattering, the path length is the geometric path length through the sample and the relationship is the Lambert–Beer law. In practice, the relationship between attenuation and absorption is nonlinear due to light scattering. An approximation is therefore needed to relate $A(\lambda)$ and $\mu_a(\lambda)$ in the presence of light scattering. The most commonly applied is the modified Lambert–Beer law [19,20]:

$$A(\lambda) = \mu_a(\lambda)d + G \quad (5)$$

where an offset *G* is used to take into account attenuation due to scattering. Alternative relationships include a parabolic model [21]:

$$A(\lambda) = -a(\mu_a(\lambda)d)^2 + b\mu_a(\lambda)d + G \quad (6)$$

where a and b are fitting parameters, as well as a power law model derived from photon diffusion theory [22]:

$$A(\lambda) = a\mu_a^{\frac{1}{2}}(\lambda) + G \tag{7}$$

Here, a model is applied based on the power law approximation [18]:

$$A(\lambda) = a\mu_a^b(\lambda) + G \tag{8}$$

where a and b are fitting parameters. It should be noted that when $b = 1$, this equation is same as the modified Lambert–Beer Law (Equation (5)) and when $b = 0.5$ the equation becomes the power law model described in Equation (7). Using Equation (8) to fit to the measured data and applying Equations (3) and (2) enabled images of oxygen saturation to be obtained. The fit is performed with a nonlinear search algorithm that uses the simplex search method [18,23]. This is a direct search method that does not use numerical or analytic gradients. For n unknown parameters of the fitting equation, the simplex in n -dimensional space is characterized by the $n + 1$ distinct vectors that are its vertices. At each step of the search, a new point in or near the current simplex is generated. The function’s value at the new point is compared with its values at the vertices of the simplex, and usually one of the vertices is replaced by the new point, giving a new simplex. This step is repeated until the diameter of the simplex is less than the specified tolerance. The fitting algorithm and model have been previously validated using Monte Carlo data that simulate light propagation in tissue [18]. In the presence of noise, this method was found to be robust and was subsequently applied to tissue measurement.

Similar to [9], tissue oxygenation was assessed by HSI at a site measuring 1 cm² in an area of intact skin adjacent (typically 1–5 mm) to the edge of the ulcer and unaffected by callus.

2.4. Principal Component Analysis

The method applied in the wound study follows a similar approach to that described in the literature for applications in the food industry [11–13]. A cropped region of interest of 50 × 50 pixels was selected, as this was found to be sufficient to extract the wound and surrounding tissue for all the images obtained. Where background pixels remained in the image (e.g., when a wound was close to or on a toe), these were removed by thresholding, as the attenuation of the background was lower than that of tissue.

The process of converting the three-dimensional data cube into images of each of the principal components is shown in Figure 2. The data cube is first unfolded into a two-dimensional matrix, where each column represents all pixels contained in one spectral band of the original image cube and each row represents each pixel’s spectrum (Figure 2). Mathematically this is expressed as [24]:

$$A_i = [A(\lambda_i)_1, A(\lambda_i)_2, \dots, A(\lambda_i)_N]_i^T \tag{9}$$

where N is the total number of pixels in the image, $A(\lambda_i)$ is the attenuation at each pixel, i represents the wavelength bin number of the spectrum, and T denotes the transpose.

To calculate the principal components, it is necessary to calculate the eigenvectors and eigenvalues of the 2D matrix (Figure 2c). The mean vector is given by:

$$m = \frac{1}{N} \sum_{i=1}^N A_i \tag{10}$$

The covariance matrix of A_i is expressed as:

$$Cov(A) = \frac{1}{N} \sum_{i=1}^N (A_i - m)(A_i - m)^T \tag{11}$$

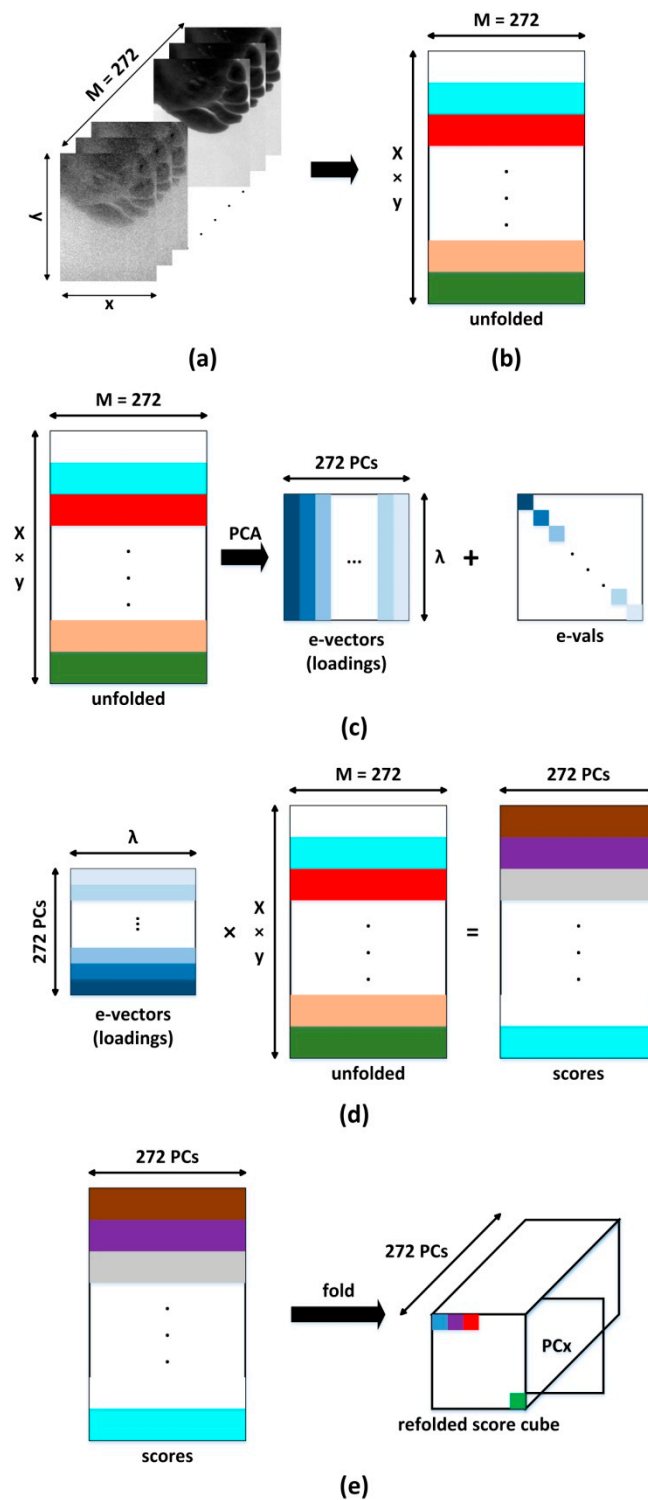


Figure 2. Principal component analysis (PCA) applied to a hypercube, where e-vector means eigenvector and e-value means eigenvalue: unfold (a) 3-D datacube into (b) 2-D matrix; (c) obtain eigenvectors and eigenvalues from covariance matrix; (d) multiply the 2-D matrix by the eigenvectors to obtain a score matrix; (e) refold the score matrix to form images at each principal component.

PCA is dependent on the eigenvalue decomposition of the covariance matrix, and $Cov(x)$ can be denoted in another form as:

$$Cov(A) = UDU^T \tag{12}$$

$$D = \text{diag} (P_1, P_2, \dots, P_N) \quad (13)$$

$$U = (u_1, u_2, \dots, u_N) \quad (14)$$

where D is the diagonal matrix, P is the eigenvalues of the covariance matrix, and U is the orthonormal matrix that contains the eigenvectors of the covariance matrix.

Multiplying the 2-D matrix A_i by the eigenvector matrix provides a score matrix v_i (Figure 2d), which can then be refolded to form a data cube that represents images of principal components.

$$v_i = U^T A_i \quad (i = 1, 2, \dots, M) \quad (15)$$

Arranging these images according to the magnitude of the eigenvector ($P_1 \gg P_2 \gg \dots \gg P_N$) enables data reduction, as usually only information is contained in the first few principal components. In this case, the oxy- and deoxyhemoglobin spectra are correlated and only the first two principal components (PC1 and PC2) are used for image classification.

In order to compare the classification performance of using SpO₂ values or PCA, receiver operating characteristic (ROC) curves are used to express the performance of a binary classifier system due to a varying discrimination threshold. An ROC curve is obtained by plotting true positive rate (TPR) against false positive rate (FPR). TPR is the fraction of true positives out of the total actual positives. FPR is the fraction of false positives out of the total actual negatives.

3. Results

A total of 43 volunteers participated in the clinical study, as previously reported [9]. There were 12 women and 31 men; mean age was 62.7 years. Six of the 43 patients had type 1 diabetes and 37 had type 2 diabetes; 9 were smokers and 39 patients were judged to have neuropathy. Median (range) ankle brachial pressure index (ABPI) was 1.06 (0.15–1.63). Median (range) estimated duration of ulcers prior to assessment was 4.97 (1–26) weeks. 24 healed by 12 weeks and a further 7 healed between 12 and 24 weeks. Ten ulcers did not heal within 24 weeks of follow-up.

3.1. Oxygen Saturation Analysis

As previously reported [9], the SpO₂ results from baseline were significantly different between ulcers that did and did not heal within 12 weeks, but not between those that did and did not by 24 weeks. Figure 3 shows measured SpO₂ at a point adjacent to the wound site against healing time (healed by 12 weeks represented by blue diamonds, unhealed at 12 weeks represented by red triangles). The dashed line shows the optimum threshold using Youden's index [25] obtained from the ROC curve shown in the next section. An R² value of 0.4 was obtained when applying a linear fit to the data obtained for healing within the first 12 weeks.

For the SpO₂ classifier with the threshold set to 59.5%, the black dashed line (shown in Figure 3) can be used as the decision line where patients with SpO₂ values adjacent to the wound site lower than the threshold are classified as healing by 12 weeks. Only two of the unhealed ulcers were grouped incorrectly. The TPR was 50.0% (12 of 24) and the FPR was 11.8% (2 of 17). When using SpO₂ values to predict the healing of diabetic ulcers in 12 weeks, the sensitivity was 50% (12 of 24), the specificity was 88.2% (15 of 17), and the positive predictive value was 85.7% (12 of 14).

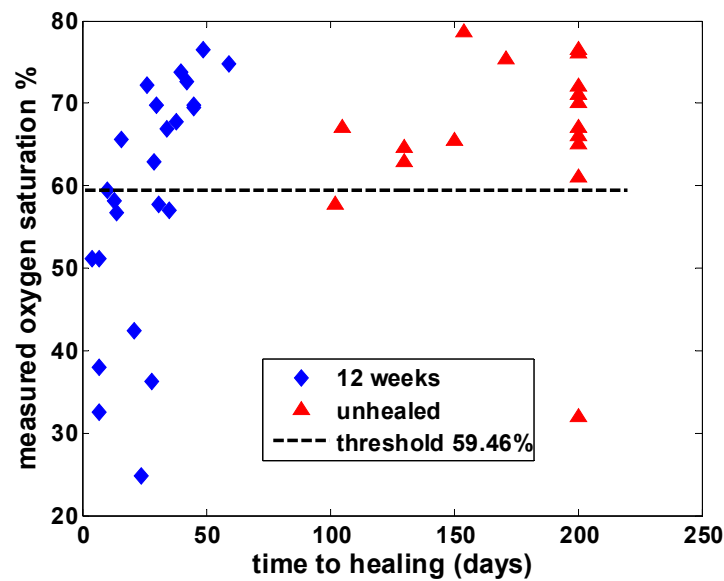


Figure 3. Relationship between time to healing (days) and oxygen saturation in a region adjacent to the wound. In order to plot unhealed ulcers, their healing days were set at 200 (higher than all the healing days of the healed ulcers). The dashed line represents the optimum threshold calculated from Youden’s index.

3.2. Principal Component Analysis

PC1 and PCs greater than 2 did not provide any indication of wound healing, so it was not possible to identify a threshold for classification of wound healing in these cases. There was, however, clustering of data corresponding to healing within 12 weeks in the second principal component (PC2) scores and thresholds could be selected. Figure 4 shows PC2 against time to healing for all patients (healed by 12 weeks represented by blue diamonds, unhealed at 12 weeks represented by red triangles). Using Youden’s index sets the upper and lower PC2 thresholds to +0.62 and -0.62. In this case, the TPR was 87.5% and the FPR was 11.8%. The sensitivity was 87.5% (21 of 24), the specificity was 88.2% (15 of 17), and the positive predictive value was 91.3% (21 of 23).

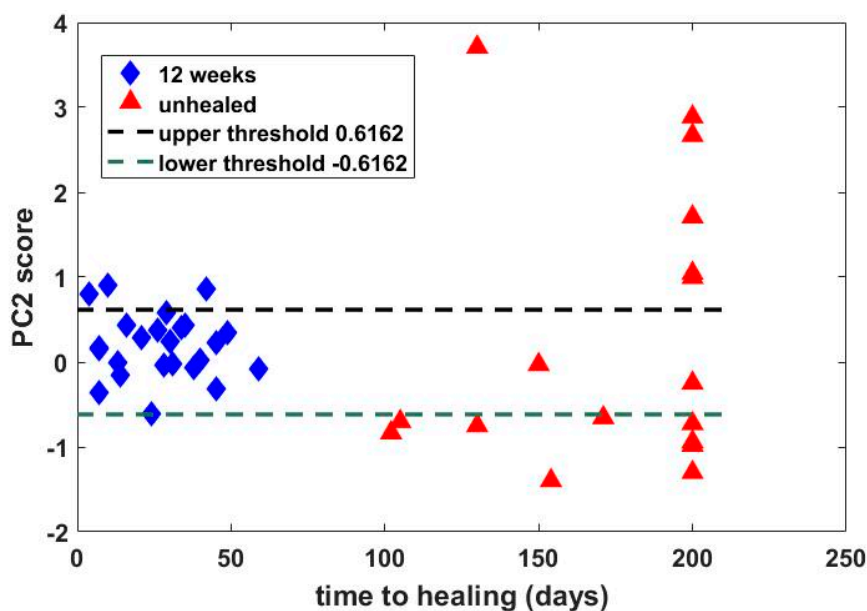


Figure 4. Relationship between time to healing (days) and principal component 2 (PC2). In order to plot unhealed ulcers, healing days was set at 200 (higher than all the healing days of the healed ulcers).

In order to further compare the performance of SpO₂ and PC2 classifiers, the ROC curve in Figure 5 shows the PCA classifier (blue line) much closer to the ideal right-angled case than the SpO₂ classifier (red line). A common method to compare classifiers in a single scalar value is to calculate the area under the ROC curve (AUC) [26]. The AUC under the PCA classifier is 0.88, which is 33% more than the AUC for the SpO₂ classifier (0.66).

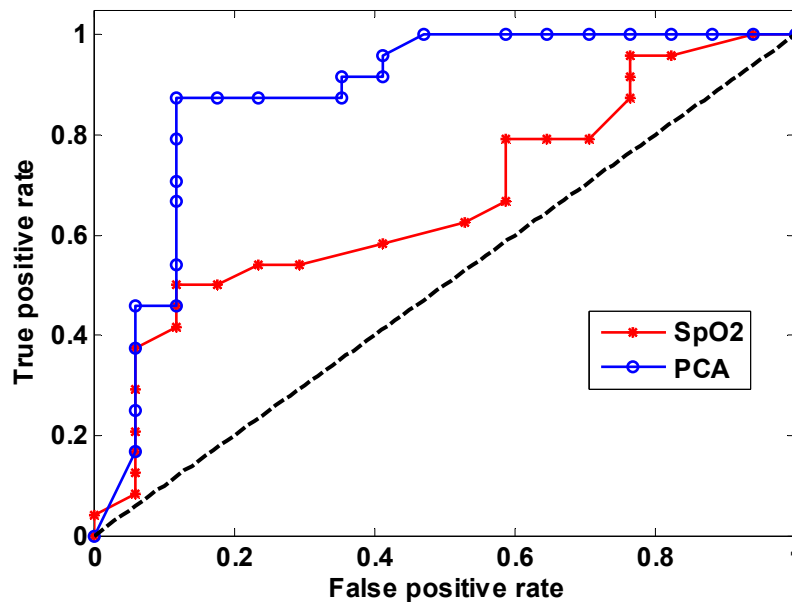


Figure 5. Receiver operating characteristic (ROC) analysis: red line indicates classification based on SpO₂ values adjacent to the wound site and blue line represents classification based on the absolute value of the PC2 score. Black dashed line is the worst case.

4. Discussion and Conclusions

Hyperspectral imaging is a tool that has the potential to predict healing of diabetic foot ulcers. Such a tool would be highly beneficial, as foot ulcers represent a major complication of diabetes and are a considerable burden for both patients and health care providers. Healing often takes many months and accurate prediction of those ulcers least likely to heal quickly can therefore be useful, because it would enable more intensive intervention at an earlier stage, which could improve overall outcome. Due to the different absorption spectra of oxy- and deoxyhemoglobin, biomedical HSI has previously predicted wound healing based on SpO₂ values. Principal component analysis is an alternative approach that has not been investigated in the prediction of wound healing. It is therefore of value to investigate whether PCA improves the prediction of wound healing and to compare this with the performance of SpO₂ mapping.

Hyperspectral images from a previous study of 43 patients with wounds were analyzed by using both SpO₂ values and PCA, and the principal finding was that classification of time to healing by 12 weeks based on PCA (sensitivity = 87.5%, specificity = 88.2%) outperformed that using SpO₂ (sensitivity = 50%, specificity = 88.2%). Comparison by receiver operating characteristic (ROC) analysis revealed an area under the curve of 0.88 for PCA, compared with 0.66 using oxygen saturation analysis. Thus, PCA based on the second principal component appeared superior to analysis using SpO₂ values in predicting healing of wounds by 12 weeks based on hyperspectral images taken at baseline.

Although one cannot uniquely map a physical property onto a principal component, it is interesting to consider how physical properties influence PCs. The absorption spectra over the range of interest (430–750 nm) are dominated by oxy- and deoxyhemoglobin. These have broadly similar features, i.e., high absorption in the blue/green region, reducing into the red/near-infrared range. We believe that these features are captured by PC1. Differences in the oxy- and deoxyhemoglobin

spectra are then characterized by PC2, which provides discrimination of wound healing with superior performance to that achieved by more widely applied SpO₂ measurement approaches. Due to the dominance of oxy- and deoxyhemoglobin, PCs greater than 2 provide no discriminatory value.

The classification performance obtained in this study is slightly better than that of our earlier publication [9] and is comparable to that obtained by another [7], which reported estimates of sensitivity and specificity of 93% and 86%, respectively, in a rather smaller group of patients. SpO₂ values may still be useful in cases where a hyperspectral camera is not available (as, for example, when making single point measurements using a lower-cost spectrometer-based method or when making measurements with a wound dressing with a fiber optic probe placed adjacent to the wound site). Furthermore, the previous demonstration that SpO₂ values on the top of the foot are well correlated with those on the underside means that precisely locating the fiber optic probe may not be necessary.

Author Contributions: Data curation, Q.Y.; Formal analysis, Q.Y., S.S., W.J.J., and F.L.G.; Funding acquisition, W.J.J.; Investigation, Q.Y., D.J.C., A.M., and S.P.M.; Methodology, W.J.J., D.J.C., F.L.G., and S.P.M.; Project administration, S.P.M.; Resources, S.P.M.; Software, Q.Y. and S.S.; Supervision, S.P.M.; Validation, Q.Y.; Visualization, S.S.; Writing—original draft, Q.Y.; Writing—review and editing, S.S., W.J.J., A.M., and S.P.M.

Funding: Q.Y. was funded by a studentship from the University of Nottingham. The original clinical study was funded by the UK National Institute for Health Research (NEAT/i4i) programme grant FSG027, and Nottingham University Hospitals Trust acted as sponsor.

Acknowledgments: We thank Nada Savic for her contribution to the original analysis and helpful discussion.

Conflicts of Interest: The authors declare no conflict of interest.

References

1. Boulton, A.J.; Vileikyte, L.; Ragnarsson-Tennvall, G.; Apelqvist, J. The global burden of diabetic foot disease. *Lancet* **2005**, *366*, 1719–1724. [[CrossRef](#)]
2. Johnson, W.R.; Humayun, M.; Bearman, G.; Wilson, D.W.; Fink, W. Snapshot hyperspectral imaging in ophthalmology. *J. Biomed. Opt.* **2007**, *12*, 014036. [[CrossRef](#)]
3. Gao, L.; Smith, R.T.; Tkaczyk, T.S. Snapshot hyperspectral retinal camera with the Image Mapping Spectrometer (IMS). *Biomed. Opt. Express* **2012**, *3*, 48–54. [[CrossRef](#)]
4. Mordant, D.J.; Al-Abboud, I.; Muyo, G.; Gorman, A.; Sallam, A.; Rodmell, P.; Crowe, J.; Morgan, S.; Ritchie, P.; Harvey, A.R.; et al. Validation of human whole blood oximetry, using a hyperspectral fundus camera with a model eye. *Investig. Ophthalmol. Vis. Sci.* **2011**, *52*, 2851–2859. [[CrossRef](#)] [[PubMed](#)]
5. Greenman, R.L.; Panasyuk, S.; Wang, X.; Lyons, T.E.; Dinh, T.; Longoria, L.; Giurini, J.M.; Freeman, J.; Khaodhiar, L.; Veves, A. Early changes in the skin microcirculation and muscle metabolism of the diabetic foot. *Lancet* **2005**, *366*, 1711–1717. [[CrossRef](#)]
6. Yudovsky, D.; Nouvong, A.; Schomacker, K.; Pilon, L. Assessing diabetic foot ulcer development risk with hyperspectral tissue oximetry. *J. Biomed. Opt.* **2011**, *16*, 026009. [[CrossRef](#)] [[PubMed](#)]
7. Khaodhiar, L.; Dinh, T.; Schomacker, K.T.; Panasyuk, S.V.; Freeman, J.E.; Lew, R.; Vo, T.; Panasyuk, A.A.; Lima, C.; Giurini, J.M.; et al. The use of medical hyperspectral technology to evaluate microcirculatory changes in diabetic foot ulcers and to predict clinical outcomes. *Diabetes Care* **2007**, *30*, 903–910. [[CrossRef](#)]
8. Nouvong, A.; Hoogwerf, B.; Mohler, E.; Davis, B.; Tajaddini, A.; Medenilla, E. Evaluation of diabetic foot ulcer healing with hyperspectral imaging of oxyhaemoglobin and deoxyhaemoglobin. *Diabetes Care* **2009**, *32*, 2056–2061. [[CrossRef](#)]
9. Jeffcoate, W.J.; Clark, D.J.; Savic, N.; Rodmell, P.I.; Hinchliffe, R.J.; Musgrove, A.; Game, F.L. Use of HSI to measure oxygen saturation in the lower limb and its correlation with healing of foot ulcers in diabetes. *Diabet. Med.* **2015**, *32*, 798–802. [[CrossRef](#)]
10. Koonsanit, K.; Jaruskulchai, C.; Eiumnoh, A. Band Selection for Hyperspectral Imagery with PCA-MIG. In *Web-Age Information Management*; Springer: Berlin/Heidelberg, Germany, 2012; pp. 119–127.
11. Kelman, T.; Ren, J.; Marshall, S. Effective classification of Chinese tea samples in hyperspectral imaging. *Artif. Intell. Res.* **2013**, *2*, 87. [[CrossRef](#)]

12. Gowen, A.A.; O'Donnell, C.P.; Taghizadeh, M.; Cullen, P.J.; Frias, J.M.; Downey, G. Hyperspectral imaging combined with principal component analysis for bruise damage detection on white mushrooms (*Agaricus bisporus*). *J. Chemom.* **2008**, *22*, 259–267. [[CrossRef](#)]
13. Liu, L.; Ngadi, M.O. Computerized pork quality evaluation system. In *Medical Biometrics*; Springer: Berlin/Heidelberg, Germany, 2010; pp. 145–152.
14. Lu, G.; Fei, B. Medical hyperspectral imaging: A review. *J. Biomed. Opt.* **2014**, *19*, 10901. [[CrossRef](#)] [[PubMed](#)]
15. Zuzak, K.J.; Naik, S.C.; Alexandrakis, G.; Hawkins, D.; Behbehani, K.; Livingston, E.H. Characterization of a Near-Infrared Laparoscopic Hyperspectral Imaging System for Minimally Invasive Surgery. *Anal. Chem.* **2007**, *79*, 4709–4715. [[CrossRef](#)] [[PubMed](#)]
16. Gerstner, A.O.H.; Laffers, W.; Bootz, F.; Farkas, D.L.; Martin, R.; Bendix, J.; Thies, B. Hyperspectral imaging of mucosal surfaces in patients. *J. Biophotonics* **2012**, *5*, 255–262. [[CrossRef](#)] [[PubMed](#)]
17. Rajpoot, K.M.; Rajpoot, N.M. Wavelet based segmentation of hyperspectral colon tissue imagery. In Proceedings of the 7th International Multi Topic Conference, Islamabad, Pakistan, 8–9 December 2003; pp. 38–43.
18. Rodmell, P.I. A Novel Oximeter. Ph.D. Thesis, University of Nottingham, Nottingham, UK, 2005.
19. Lübbers, D.W.; Wodick, R. The examination of multicomponent systems in biological materials by means of a rapid scanning photometer. *Appl. Opt.* **1969**, *8*, 1055–1062. [[CrossRef](#)] [[PubMed](#)]
20. Stockford, I.M.; Lu, B.; Crowe, J.A.; Morgan, S.P.; Morris, D.E. Reduction of Error in spectrophotometry of scattering media using polarization techniques. *Appl. Spectrosc.* **2007**, *61*, 1379–1389. [[CrossRef](#)] [[PubMed](#)]
21. Loyalka, S.; Riggs, C. Inverse problem in diffuse reflectance spectroscopy: Accuracy of the Kubelka-Munk equations. *Appl. Spectrosc.* **1995**, *49*, 1107–1110. [[CrossRef](#)]
22. Arridge, S.R.; Cope, M.; Delpy, D. The theoretical basis for the determination of optical pathlengths in tissue: Temporal and frequency analysis. *Phys. Med. Biol.* **1992**, *37*, 1531. [[CrossRef](#)]
23. Lagarias, J.C.; Wright, J.A.R.M.H.; Wright, P.E. Convergence properties of the nelder-mead simplex method in low dimensions. *SIAM J. Optim.* **1998**, *9*, 112–147. [[CrossRef](#)]
24. Gonzales, R.C.; Woods, R.E. *Digital Image Processing*, 2nd ed.; Prentice Hall: Upper Saddle River, NJ, USA, 2002.
25. Fluss, R.; Farragi, D.; Resiser, B. Estimation of the Youden Index and its associated cutoff point. *Biom. J.* **2005**, *47*, 458–472. [[CrossRef](#)]
26. Fawcett, T. An introduction to ROC analysis. *Pattern Recognit. Lett.* **2006**, *27*, 861–874. [[CrossRef](#)]



© 2018 by the authors. Licensee MDPI, Basel, Switzerland. This article is an open access article distributed under the terms and conditions of the Creative Commons Attribution (CC BY) license (<http://creativecommons.org/licenses/by/4.0/>).